Supplementary Materials: ***MYBPC3*** **Mutations cause Hypertrophic Cardiomyopathy by Dysregulating Myosin: Implications for Therapy**

Christopher N. Toepfer[1,2,3*], Hiroko Wakimoto[1,4], Amanda C. Garfinkel[1], Barbara McDonough[1], Dan Liao[5], Jianming Jiang[5], Angela Tai[1], Josh Gorham[1], Ida G. Lunde[1,6], Mingyue Lun[7], Thomas L. Lynch IV[8], Sakthivel Sadayappan[9], Charles S. Redwood[2], Hugh Watkins[2,3], Jonathan Seidman[1], Christine Seidman[1,10,*]

Supplementary Materials and Methods:

Quantification of cMyBPC protein levels in MYBPC3 variant mouse models
MyBPC was depleted in the hearts of mice by injection of MyBPC-RNAi at post-natal day 10 and by germline mutations in *Mybpc3* mutations that inserted the PKG-neomycin resistance gene insertion into one or both copies of exon 30. The resultant protein is truncated from 1270 amino acids to 1064 amino acids (Supplemental Figure 1A). Western blots of cardiac tissues demonstrate reduced cMyBPC levels in the MyBPC-RNAi and Mybpc3$^{t/+}$ and Mybpc3$^{t/t}$ mice (Supplemental figure 1B). Densitometry of these blots indicated that cMyBPC protein levels were ~35 ± 8% (Mybpc3$^{t/+}$) and ~13 ± 7% (Mybpc3$^{t/t}$) and absent in RNAi- treated mice (Supplemental Figure 1C).

In vivo comparisons of *Mybpc3* mouse models
Echocardiography of Mypbc3$^{t/+}$ and MyBPC-RNAi mice (Supplemental Figure 2A) showed comparable fractional shortening (FS) to wildtype (WT) and sham-injected mice across study ages (5-20 weeks). By contrast fractional shortening of the DCM model, Myh6$^{F764L/\ F764L}$ is reduced. MyBPC-RNAi and Myh6$^{F764L/\ F764L}$ mice have hypertrophy (increased left ventricular posterior wall thickness; LVPWT) unlike WT and Mybpc3$^{t/+}$ mice across all ages studied (5-20 weeks) in agreement with previously published increases in LVPW of Mybpc3$^{t/t}$ mice[23, 25, 33](Supplemental Figure 2B). MyBPC-RNAi reduced cMyBPC RNA levels < 10% of sham control (Supplemental Figure 2C).

Characterization of viral titers for Mybpc3 expression depletion
Assessments of Mybpc3 expression were performed and normalized to beta actin in response to increasing viral titers of MyBPC-RNAi virus (Supplemental Figure 3A). *In vivo* measurement of left ventricular posterior wall thickness (LVPW) showed that increasing viral titer resulted in hypertrophy (increased LVPW) (Supplemental Figure 3B).

Assessing fluorescent decay in Mant-ATP experiments
By measuring fluorescent intensity decay over multiple sections of chemically permeabilized myocardium we assessed the ratio between the amplitudes of the fast and slow decays of a double exponential fluorescent decay (Supplemental Figure 4A). We provide a movie of this decay in a section of skinned myocardium that has been imaged as indicated in the methods section (Supplemental Figure 4B)

Mant-ATP control measures to control for hypertrophy or myosin DCM on assay findings
Mant-ATP assays performed on permeabilized myocardium Myh6$^{764/764}$ mice showed no change in SRX and DRX ratios (Supplemental Figure 5). As this DCM mutation in myosin depresses sarcomere contraction without altering relaxation, we deduced that the improved contractility and relaxation in in Myh6$^{764/764}$ mice treated with MyBPC-RNAi reflects repression of myosin's motor function (Supplemental Figure 5).

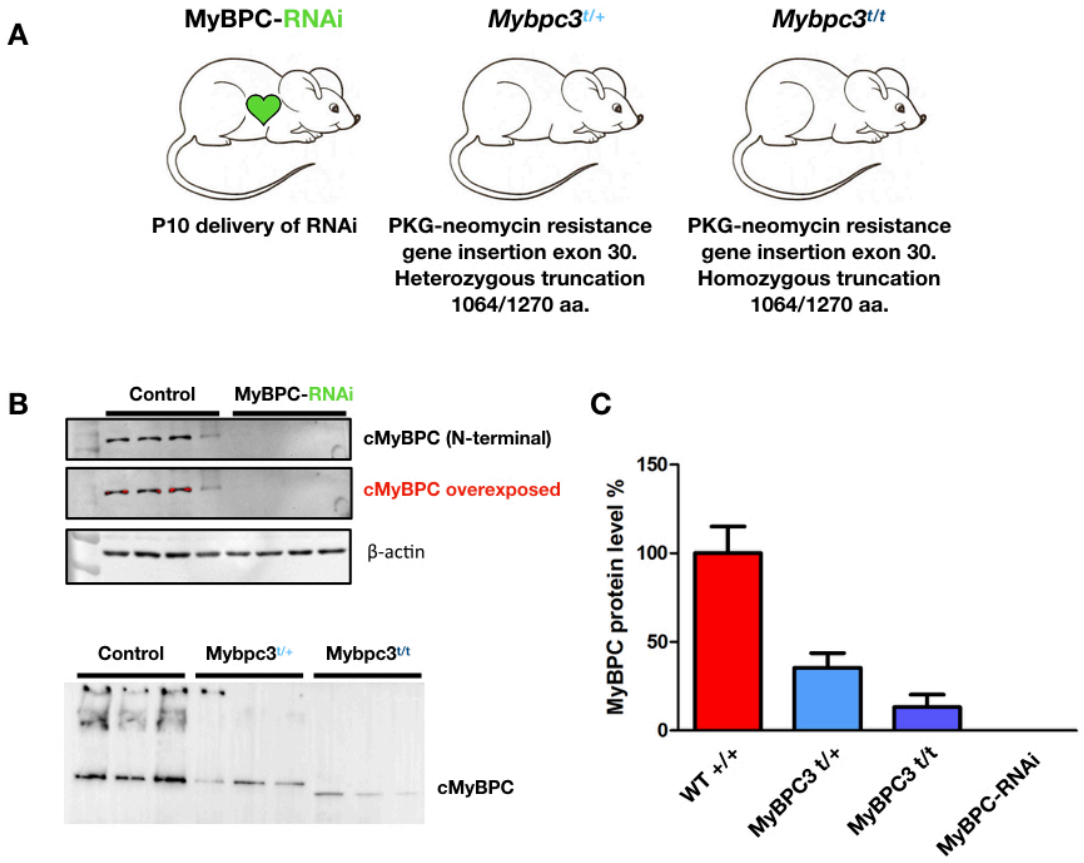

Supplemental figure 1: *Mybpc3* mouse models. A) Pictorial representation and description of murine models used to assess cMyBPC deficiency on cellular function. **B)** Western blots of cMyBPC extracted from the myocardium of MyBPC-RNAi (top) and from Mybpc$^{t/+}$ and Mybpc$^{t/t}$ mice demonstrates reduces cMyBPC protein expression. **C)** Densitometry of blots quantifies the reduction of cMyBPC in each genotype.

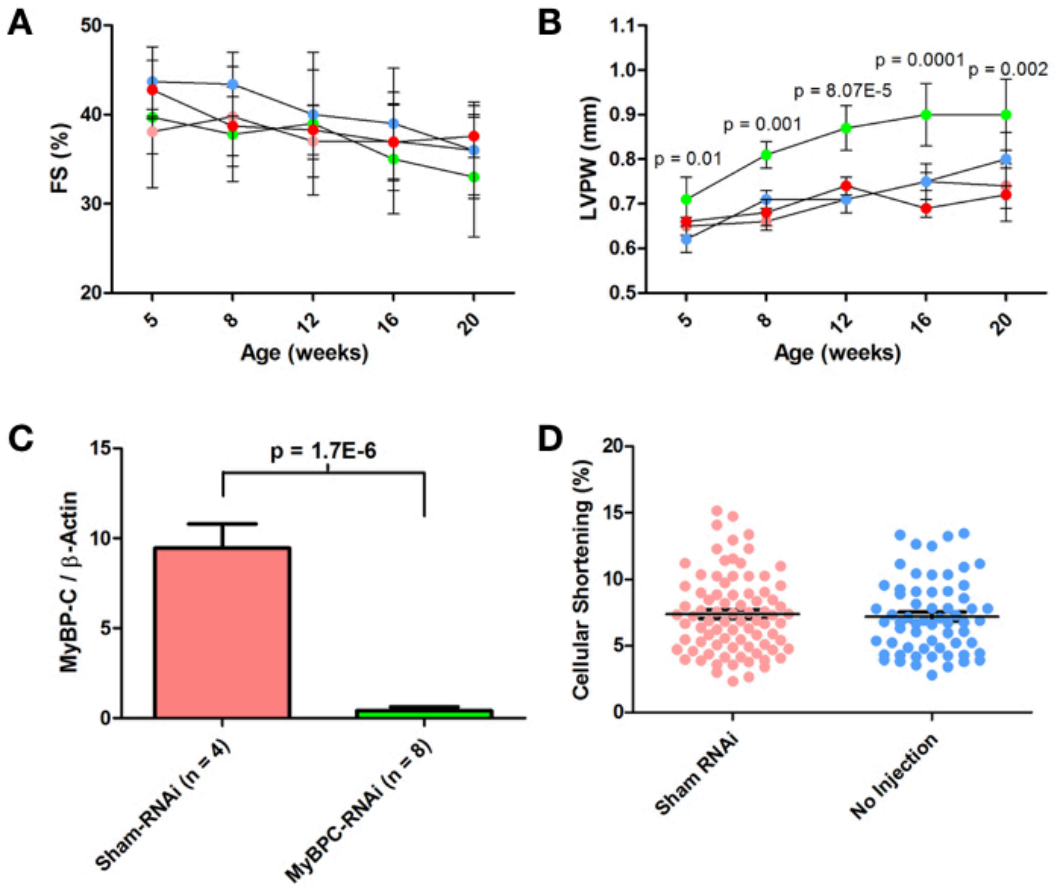

Supplemental Figure 2: *In vivo* cardiac function and proteomic characterization in MyBPC models. A) Fractional shortening of mouse genotypes including MyBPC-RNAi (Green, n=8), Mypbc3$^{t/+}$ (Blue, n=4) , Sham-RNAi of Mypbc3$^{t/+}$ (Pink, n=4) , and WT (Red, n=4) as a function of age (weeks). **B)** Left ventricular posterior wall thickness (LVPW) of mice as a function of age (weeks). **C)** Levels of cardiac tissue *Mybpc3* RNA in comparison to β-actin in Sham-RNAi and MyBPC-RNAi mice. **D)** Cellular shortening, a measure of contractility in Sham-RNAi (no Mybpc3-RNAi) and Mypbc3$^{t/+}$ mice shows no effect of vector injection on contractility.

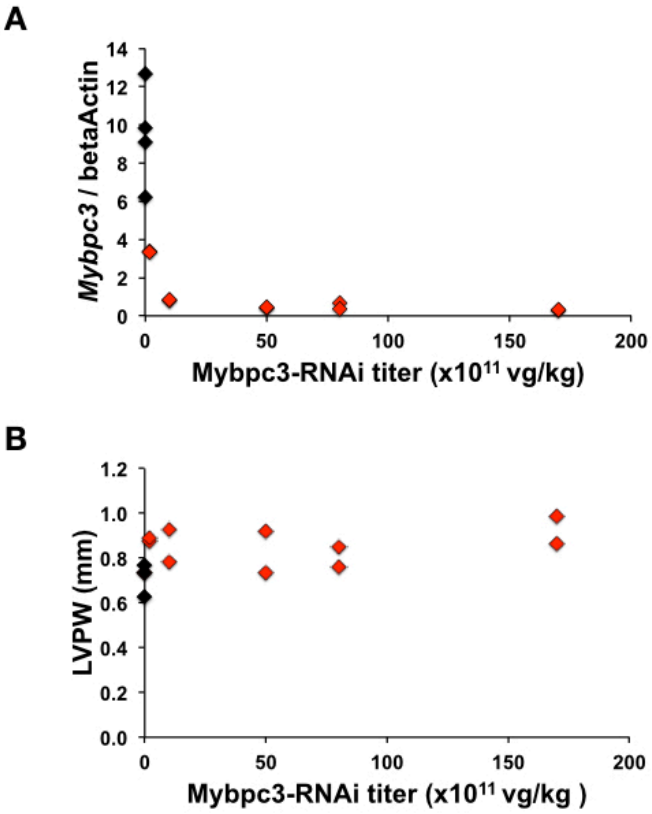

Supplemental Figure 3: The protein and function effects of increasing Mybpc-3-RNAi titers. A) *Mybpc3* transcripts, normalized for beta actin expression, in mice treated with increasing titers of Mybpc-3-RNAi (red diamonds) and untreated mice (black diamonds). **B)** Viral titer correlated with left ventricular posterior wall thickness (LVPW) in mice treated with Mybpc-3-RNAi (red diamonds) compared to untreated mice (black diamonds).

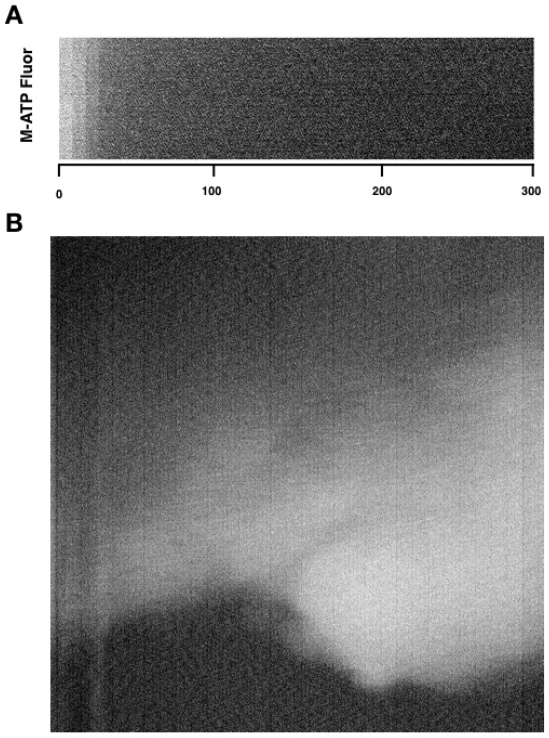

Supplemental Figure 4: Analysis of Mant-ATP video files. A) Representative fluorescence change per frame imaged throughout a Mant-ATP dark ATP chase, frame capture is every 10 seconds. **B)** Frame from a representative movie showing a section of myocardium during fluorescent washout, frame capture rate is once per 10 seconds and decays were imaged for 15 minutes. See Movie S1 for fluorescence washout.

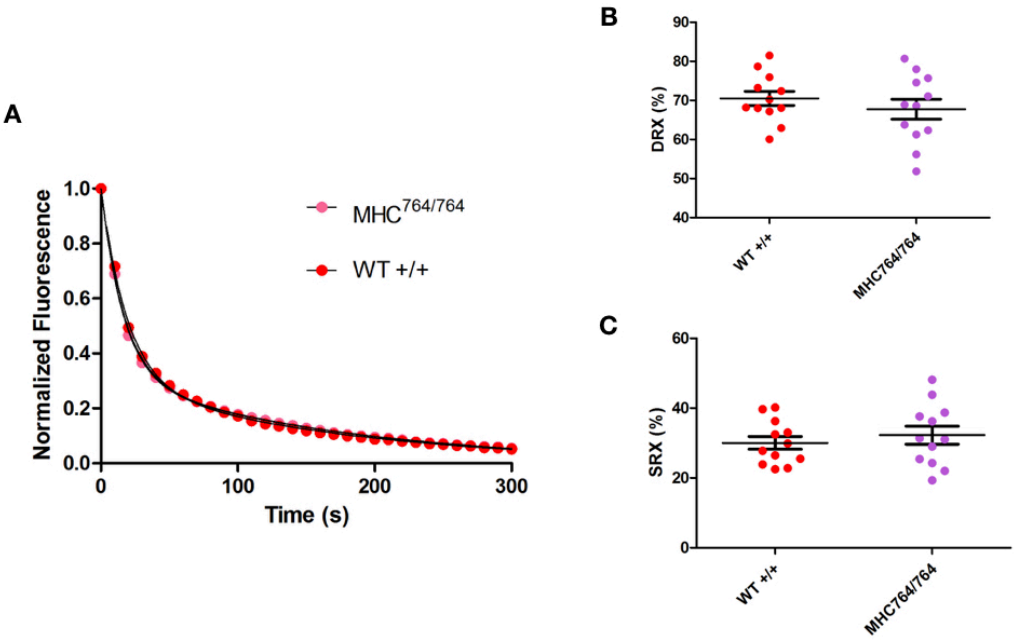

Supplemental Figure 5: Mant-ATP assays in cardiac tissues for Myh6$^{764/764}$ **mice with DCM. A)** Average Mant-ATP fluorescence decay curves of myocardium from Myh6$^{764/764}$ mice (n= 3, with 12 experiments per mouse). Data is fit by double exponential decay to assess ratios of DRX and SRX heads in the myocardium. **B)** Plot of the initial rapid decay amplitude corresponding to DRX heads. Data are plot with mean ± SEM indicated. **C)** Plot of the second exponents of slow decay amplitude corresponding to SRX heads. Data are plot with mean ± SEM indicated. All significances are indicated with corresponding p values.

Supplemental Movie S1: The fluorescent decay during dark ATP chase of Mant-ATP in permeabilized myocardium. A single frame is provided in Supplemental figure 4B.